Design, Construction, and Performance of the Leighton 10.4-m-Diameter Radio Telescopes

DAVID WOODY, MEMBER, IEEE, DAVID VAIL, AND WALTER SCHAAL

Invited Paper

The design, construction, and measurement of 10-m-class radio telescopes operating at millimeter and submillimeter wavelengths present many difficult challenges. The radio telescopes developed by Robert Leighton provide an economical solution to these problems. These 10.4-m-diameter telescopes have diffraction-limited beams at wavelengths as short as 300 μm. This paper describes the innovative techniques Robert Leighton developed to solve many of the problems encountered in building precision telescopes. The areas covered include the design of the homologous reflector support structure, the computer program used to accurately predict the deformations of the surface as a function of gravity, wind and temperature, the construction techniques used to minimize the stress and bending moments in the structure, and the methods developed for producing and measuring a 10.4-m-diameter reflector surface to the required accuracy.

The reflectors for the Leighton telescopes consist of honeycomb aluminum panels supported on a steel spaceframe backing structure. The spaceframe utilizes precision machined members and pin joints. The 84 panels form a hexagonal tiling pattern in the aperture plane and are figured using a custom-built machine that cuts the parabolic shape into the exposed honeycomb core while all of the panels are assembled on the backing structure. The aluminum reflecting surface is then applied to the front of each panel.

The techniques used to fabricate the Leighton telescopes have proven to be very successful. The telescopes are routinely fabricated and installed with an rms surface accuracy of less than 35 μm without any adjustments or corrections. The computer calculations of the homologous deformation of the telescopes as they move in elevation have been verified by holographic measurements of the aperture field pattern using astronomical sources. The telescopes have survived 15 years of operation in the 1200-m altitude desert site at the Owens Valley Radio Observatory with no evidence of degradation. A Leighton telescope installed at the Caltech Submillimeter Observatory on Mauna Kea, HI, has achieved an accuracy of < 20 μm.

Manuscript received August 30, 1993; revised November 4, 1993. This work was supported in part by the National Science Foundation under Grants AST–9016404 and AST–9015755. Additional fundung was supplied by the Creske Foundation, the Oscar and Elsie Meyer Foundation, the Norris Foundation, as well as Caltech and JPL internal funds.

D. Woody is with the Division of Physics, Mathematics, and Astronomy, California Institute of Technology, Owens Valley Radio Observatory, Big Pine, CA 93513.

D. Vail and W. Schaal are with the Division of Physics, Mathematics and Astronomy, California Institute of Technology, Department of Physics, M.S. 320-47, Pasadena, CA 91125.

IEEE Log Number 9400203.

I. Introduction

Astronomical observations at wavelengths from 0.3 to 3 mm have proven very useful in the study of astronomical objects ranging from planetary atmospheres to diffuse giant molecular clouds in distant galaxies. The rotational transitions of many of the molecules of interest in astrophysics occur in this millimeter/submillimeter band. Information about the chemistry, density, temperature, and kinematics of the objects can be learned from measurements of the emission from these molecules. Interstellar and circumstellar clouds can also be studied by measuring the continuum emission from dust at millimeter and submillimeter wavelengths. The atmospheric transmission allows observation of the longer wavelengths in this band from low elevation observatories while the shorter wavelength observations must be made from high-altitude sites or from space. The objects of interest are inherently weak and the observations require sensitive receivers and telescopes with large collecting area and a surface accuracy approaching 20 μm or better. Interferometric arrays of telescopes are required to obtain angular resolution comparable to that achieved at optical wavelengths. The design and construction of telescopes operating in the submillimeter band present many difficult challenges.

This paper describes the 10.4-m-diameter radio telescopes developed by Robert Leighton for astronomical observations at millimeter and submillimeter wavelengths [1]. Leighton started the project in 1971 with the goal of developing an economical method for fabricating 10-m-class radio telescopes with ~ 50-μm surface accuracy for diffraction-limited operation at wavelengths as short as 1 mm. To achieve this goal, the accuracy of the telescopes would have to approach the physical limits set by gravity and the structural strength of common construction materials [2]–[4]. The project was very successful and exceeded its initial goals. The first production telescope, which was completed in 1978 as the first element of the Owens Valley Radio Observatory (OVRO) millimeter interferometer array, had a surface accuracy of 35 μm for nighttime observations.

0018–9219/94$04.00 © 1994 IEEE

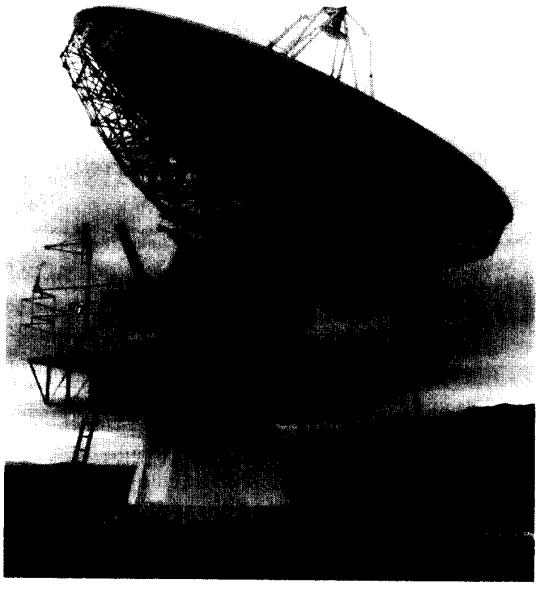

Fig. 1. One of the five Leighton telescopes in the Owens Valley millimeter interferometer array.

Currently, there are five Leighton telescopes operating in the OVRO array with a sixth telescope under construction. Figure 1 is a picture of one of the telescopes from this array. These telescopes have performed excellently in the open air at the 1200-m altitude site near Bishop, CA. All of the telescopes have achieved or exceeded the surface accuracy of the first telescope and show no signs of degradation. An additional higher-precision Leighton telescope has been in operation at the Caltech Submillimeter Observatory (CSO) located at the 4000-m level of Mauna Kea, HI, since 1986. This telescope is a slightly modified version of the telescopes used at OVRO. It is in a dome and is operated only at night. Recently, it has been adjusted to have a surface accuracy of 15–20 μm rms. This telescope achieves a diffraction-limited beam well into the submillimeter-wavelength range.

Although the Leighton design has been in use for more than 15 years, there are still many unique features that are relevant to new ground- and space-based telescopes. The structure uses precision struts and pinned joints and can be disassembled and reassembled with little loss of accuracy. The accuracy of the surface is determined by a machining fixture used to cut the honeycomb panels while they are all attached to the spaceframe backing structure. This removes the requirement of having to accurately measure and adjust the surface after the telescope is assembled in the field. Robert Leighton showed that with careful attention to details and sources of error you can reliably fabricate 10-m-size structures with an accuracy approaching one part per million. This paper is based in large part on the work in [1].

II. Synopsis

The structural design of the telescope is presented in Section III. A key feature of the design is the steel space-frame backing structure used to support the reflector panels. The spaceframe nodes form a uniform triangular grid when viewed along the optical axis. This simplifies the node design and allows an economical implementation of pin-joint construction for the spaceframe. A high degree of homology is achieved by decreasing the weight of the members which are further away from the optical axis. Another feature of the uniform triangular node pattern is that the panels form a hexagonal tiling pattern when projected onto the aperture plane. The focal length of the 10.4-m-diameter parabolic reflector is 4.12 m. The telescope has a bent Naysmith configuration with a 0.606-m-diameter hyperbolic subreflector which produces a cassegrain focal point 6.2 m away at the point where the elevation and azimuth axes intersect. A tertiary mirror at this point directs the beam along the elevation axis into the receiver cabin. The steel quadrapod supporting the subreflector is attached directly to spaceframe at approximately half the radial distance from the center to the rim of the reflector.

The computer modeling of the backing structure is described in Section IV. The program used to predict the deformation of the reflecting surface uses a relaxation algorithm which can handle nonlinear constraints. It was developed in the 1970's and has been found to agree very well with recent versions of NASTRAN. The program is used to optimize the structure for gravitational and wind distortions. The optimization goal is to minimize the deviation from the best fit paraboloid as a function of elevation, i.e., deviation from homology. The strength and play of the pin joints used in the computer model are based upon the measurements of test assemblies in the laboratory. The structure is calculated to be 92% homologous with deviations from homology of less than 17 μm rms over the full elevation range. The effect of thermal gradients and temperature changes is also calculated. The steel backing structure has a thermal time constant of less than 1/2 h. The structure is very open and is brought into thermal equilibrium with the air by winds as low as $\sim$ 5 m/s, even under asymmetric solar illumination. Thermal gradients are predicted to cause less than 25 μm rms distortion of the surface. Thermal gradients through the honeycomb panels caused by solar illumination of the front surface produces $\sim$ 25 mm rms of distortion. The net calculated distortion from gravity, wind and temperature is less than 40 μm rms for the OVRO telescopes operating in the open air during the day. This is reduced to $<$ 21 μm rms for the CSO telescope which is in a dome and used only at night.

The techniques used to fabricate the Leighton telescopes are described in Section V. Two of the salient construction techniques are the use of precision machined spaceframe members and the cutting of the reflector surface as a single monolithic structure utilizing a custom-built machining fixture. The manufactured accuracy of the $\sim$ 1-m-long spaceframe members is 10 μm. This minimizes the built-in stresses when the backing structure is assembled and allows the reflector to be disassembled and reassembled with very little loss in the surface accuracy. The backing structure is assembled on an air bearing and the aluminum

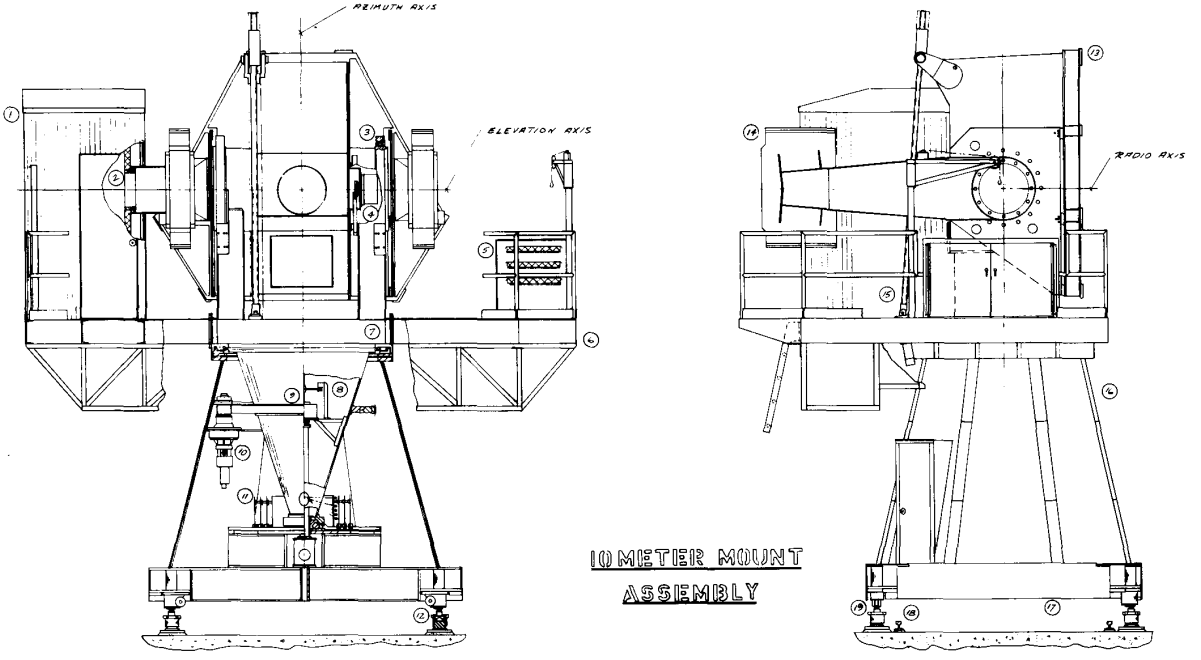

Fig. 2. Drawing of the telescope mount. Key: 1) receiver room, 2) receiver plate, 3) elevation bearing, 4) elevation encoder, 5) helium compressor for 4 K closed-cycle refrigerators, 6) compressor platform, 7) alidade platform, 8) tiltmeters, 9) azimuth encoder, 10) azimuth drive motors, 11) azimuth cable wrap, 12) tie-down nuts, 13) reflector mounting platform, 14) counter weight, 15) elevation drive ball screw, 16) insulated pedestal, 17) clearance for antenna transporter, 18) transporter rails, 19) positioning peep sight.

honeycomb panels, minus their front skin, are attached. The reflector surface is figured by machining the desired parabolic shape directly into the exposed honeycomb core of the panels using a cutter riding on a precision parabolic track as the reflector is rotated on the air bearing. 1-mm-thick aluminum sheet is then epoxied to the cut honeycomb panels to form the actual reflecting surface. This process works very well and the worst case fabrication error based on measurements of the six antennas built so far is 24μm rms.

The measurement of the reflector surface is an important part of constructing and installing a precision radio telescope. The measurement techniques and results are discussed Section VI. The methods used range from transducer measurements in the laboratory to holographic maps of the aperture plane phase using the planets and strong Quasars as radiation sources. The combination of these techniques measures the surface figure on scale sizes greater than 40 mm with an accuracy of $\sim$5 μm. The holographic maps measure the net performance of the telescope, including the subreflector and beam transport optics, under the same conditions that the astronomical observations are made. The measured performance indicates that the Leighton telescopes meet the goal of achieving a surface accuracy of better than 50 μm during exposed daytime operation in the OVRO millimeter array and better than 20 μm for the CSO telescope operating in an open dome at night.

III. Telescope Geometry

The 10.4-m-diameter reflecting surface of the Leighton telescope consists of laminated honeycomb aluminum panels supported on a tubular steel spaceframe backing structure. The backing structure, in turn, is attached to the alt–az mount drawn in Fig. 2. The mount is counterweighted and utilizes a ball–screw elevation drive. The azimuth axis is defined by a hemispherical tail bearing near ground level to take the vertical load and radial thrust rollers on a 2.21-m-diameter ring 2.29 m above the tail bearing. The azimuth drive consists of two drive motors and planetary speed reducers driving a 1.74-m-diameter bull-gear. The motors are biased in opposite direction to provide the preload to the azimuth drive system. A Naysmith optical configuration is utilized consisting of the parabolic primary, hyperbolic secondary and an ellipsoidal tertiary at the intersection of the elevation and azimuth axes. The radio beam then passes through the 0.5-m clear aperture of one of the elevation bearings into the receiver cabin.

The dish mount and backing structure are bolted together at nine points which lie in a plane parallel to the antenna aperture. The mount and antenna surface are manufactured and tested separately and then combined at the site where the antenna will be used. The rest of this paper will concentrate on the design, construction, and performance of the reflector surface and backing structure.

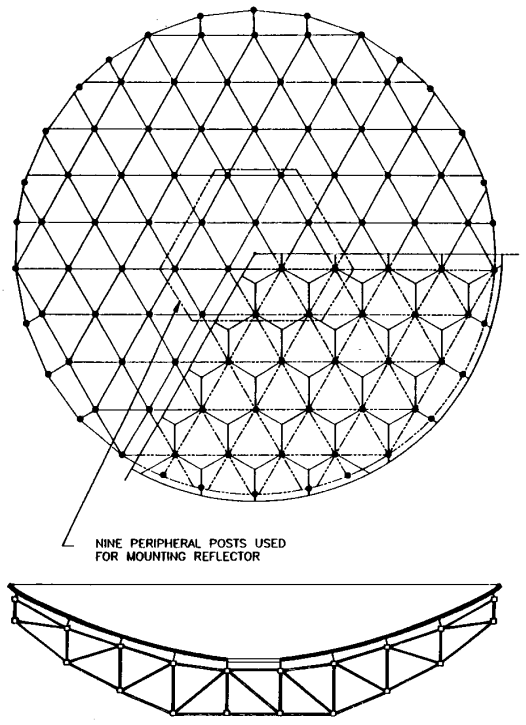

Fig. 3. Plan view and cross section of the spaceframe backing structure and panels.

The design and construction of the backing structure are the most important factors in determining the deformation of the reflector surface under different environmental conditions and gravitional forces. The guiding principal for designing the backing structure was to produce a spaceframe structure with a high degree of homogeneity and isotropy so that it will deform homologously under gravitational loading. In addition, a very open spaceframe was desired so that even in light winds it would remain in thermal equilibrium with the air. Another constraint on the design was that the spaceframe nodes be fairly simple and easy to construct.

Figure 3 shows a plan view and cross section of the reflector surface and spaceframe. The telescope backing structure consists of two sets of nodes which are laid out in a regular triangular grid when viewed along the optical axis. The front set of nodes lie on a parabolic surface with the same focal length as the desired front surface. The back nodes also lie on a paraboloid. The front and back nodes are aligned on the same triangular grid and are connected by posts which are oriented parallel to the optical axis. The paraboloid for the back nodes is truncated in a plane where the backing structure attaches to the mount. The nine nodes which are bolted to the mount are indicated in Fig. 3. The front and back ends of neighboring posts are connected by front, back, and diagonal struts for complete triangulation of the spaceframe.

Only a few parameters are required to specify the spaceframe node positions, starting with the telescope diameter of 10.4 m and focal length of 4.12 m. The triangular grid unit length is 1.143 m. The back node paraboloid is defined by the untruncated spaceframe depth at the rim and on the optical axis of 0.508 and 1.270 m, respectively. The outer six of the attachment nodes define the truncation of the back node paraboloid for attachment to the mount.

An important aspect in constructing the backing structure is the node design and the method used to attach the structural members to the nodes. This determines how difficult it is to manufacture the space frame and plays a critical role in determining its ultimate performance. As many as ten members meet at a node and they must all be attached so that the lines of force intersect at the node point. This should be achieved with a minimum of excess weight and cost.

The spaceframe geometry described above lends itself to an elegant solution of the node design problem. All of the post members are parallel to the optical axis and located on the equilateral triangular grid pattern in the aperture plane. The nodes at the ends of the posts consist of six equally spaced fins oriented parallel to the posts. The fin assemblies are referred to as spiders which are rigidly fastened to the posts. The struts connecting neighboring posts have slotted ends and are pinned to the fins as shown in Figs. 4 and 5. The attachment holes in the spider fins are placed so that the lines of force all intersect at the node point in the center of the spider.

The spaceframe is divided into concentric hexagonal rings which are assigned different weight and stiffness classes. Table 1 lists the cross sections and material used for the different classes of posts, struts, and spiders. The dimensions were chosen to correspond to commercially available stock. The backing structure has a total of 216 nodes connected by 108 axially aligned posts and 774 lateral and diagonal struts. The net weight of the spaceframe is 3600 kg.

The secondary mirror at the prime focus is supported by feedlegs attached to the backing structure 2.69 m from the optical axis. Most of the weight is carried by the legs in the plane perpendicular to the elevation axis. The legs in the plane of the elevation axis are light-weight and only handle the wind loading on the secondary structure. The secondary and feedlegs have a total weight of 310 kg.

The panel outlines are elongated hexagons which form a hexagonal tiling pattern when viewed along the optical axis as shown in Fig. 3. There are 84 panels with 10 different outlines, four of which have left- and right-hand versions. The corners of all of the panels are fastened together where they meet. This strengthens the structure and minimizes the step discontinuities between panels as the antenna is stressed. Half of the corners lie directly above a backing structure node and are attached to that node via a single 150-mm-long standoff as shown in Figs. 4 and 5. The other half of the corners, referred to as neutral corners, fall in the middle of the triangular grid and are not attached to backing structure. The adjustment of a standoff moves the corners of the three panels meeting at that point together. Thus the panels essentially form a continuous membrane which is

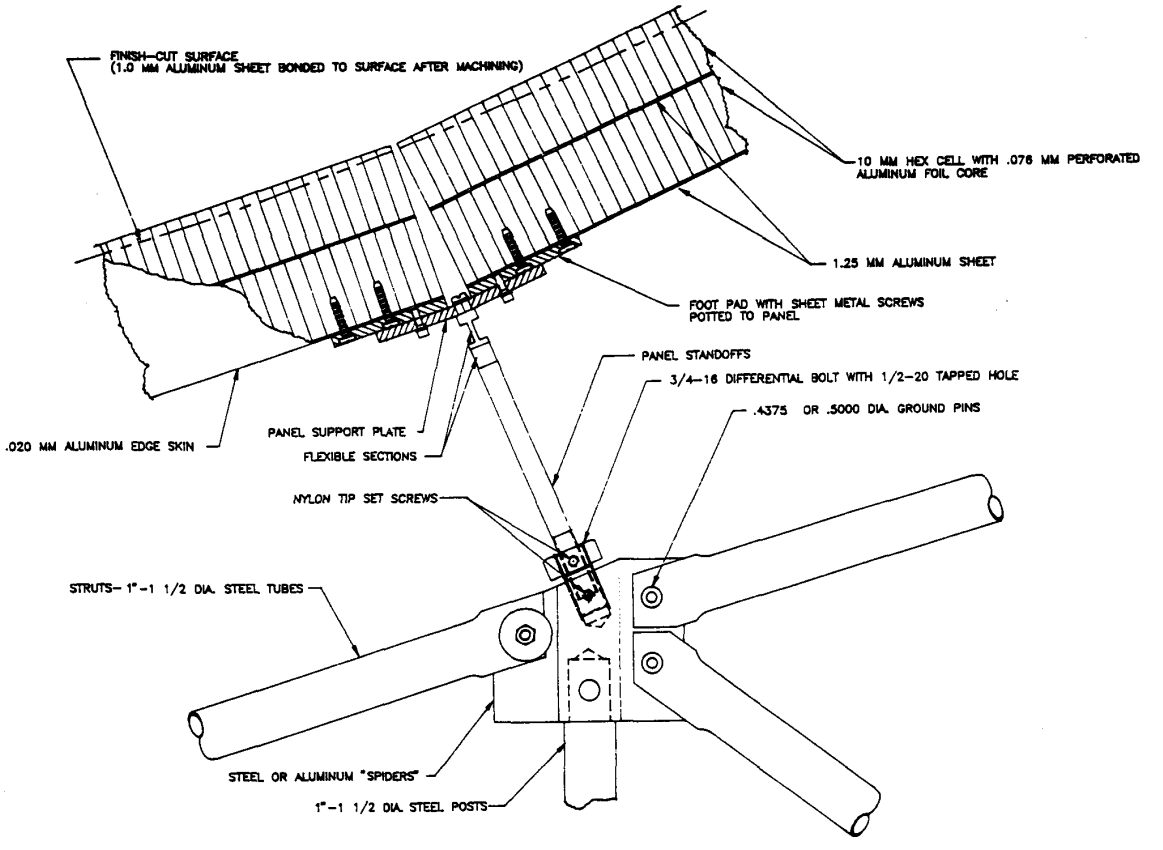

Fig. 4. Schematic drawing showing a typical spaceframe node, the honeycomb aluminum panel cross section, and the method for attaching the panels to the backing structure.

Table 1 Specifications for Spaceframe Weight Classes

Class	Posts	Struts	Spiders
I	38.1 mm dia solid, 1018 steel	38.1 mm dia × 7.1 mm wall*	9.5 mm fins, brazed steel
II	31.8 mm dia × 9.5 mm wall**	38.1 mm dia × 7.1 mm wall*	9.5 mm fins***
III	28.6 mm dia × 4.8 mm wall**	31.8 mm dia × 4.8 mm wall*	9.5 mm fins***
IV	25.4 mm dia × 2.1 mm wall**	25.4 mm dia × 3.0 mm wall*	4.8 mm fins***

* 1018 carbon steel cold drawn seamless tubing.
** 1015 carbon steel cold drawn seamless tubing.
*** 2024-T4 aluminum extrusions.

supported at 99 points, much like a meniscus mirror. The panels are constructed from honeycomb aluminum and have an area density of 15 kg/m^2 giving a net surface weight, including panel attachment hardware, of 1300 kg.

IV. Calculated Performance

An important aspect to producing a high-quality antenna is the computer model of the structure. The simulation program used for these antennas was originally written in Fortran to run on a CDC 6400 computer in the early 1970's. It is currently running under VMS FORTRAN. An iterative relaxation method is used to calculate the deformations. This method has proven to be very efficient for the Leighton telescopes which have a nearly homogeneous backing structure consisting of pin joints arranged to produce no bending moments. This method also has the advantage that it is relatively easy to add special nonlinear conditions such as play in the joints.

The simulations are based upon the three-dimensional stiffness of each node calculated by assuming that all the other nodes are held fixed. The backing structure geometry, member cross sections, and measured joint elastic characteristics are used to calculate the stiffness matrix. The

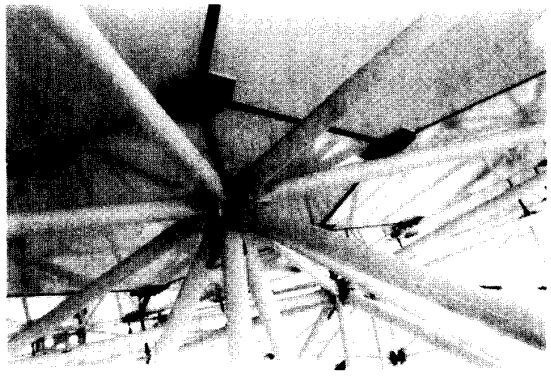

Fig. 5. Picture of the backside of the reflector surface showing a part of the spaceframe and the panel attachment method. The various components can be identified by referral to Fig. 4.

calculated net external force at each node includes gravity and wind. The gravitational force at each node is half of the weight of the connecting members plus the appropriate panel weight. At each iteration, the net force at each node is calculated as the vector sum of the post and strut internal stresses caused by their length changes, including thermal expansion, plus the external forces. The incremental displacement of each node is then calculated from the net unbalanced force and the predetermined stiffness of the node. The antenna reflector mounting platform is much stiffer than the backing structure and the nodes at the nine attachment points are restrained to fixed positions with the unbalanced forces at these nodes being taken up by the mount. The new node positions are used to calculate the length change and associated stress in each spaceframe member and the next iteration is started. Initially the nodes are at their nominal positions with no internal stress on the members, i.e. perfect member lengths. The calculations are iterated until the largest unbalanced force and rms of the unbalanced forces satisfy predetermined criteria, typically 1.5 and 0.5 N, respectively. It typically takes one to two thousand iterations to satisfy these criteria. Damping factors can be added for the calculated displacement if the iterations do not converge smoothly or feed forward can be applied to speed the convergence of well-behaved structures.

The elasticity and strength of each class of strut-to-spider-pin connection was measured in the laboratory and included in the model as an effective extra strut length when the stress is calculated. The effective extra length varies from 100 to 250 mm. One of the special joint conditions included in the model is play in the pin joints. Most of the joints are epoxied and have no play, but 20% are left dry so that the backing structure can be disassembled for shipping. The joints consist of precision reamed holes and ground pins and a play of 5 μm is used for the unepoxied joints. The play in these joints is included in the calculation of the force at a node arising from a length change in a strut, i.e., the struts stress is zero if the length change is less than the play.

The panels, feedlegs, and secondary mirror system are treated as dead weight. The stiffness of the membrane created when the panels are connected together at their corners and the stiffness of the feedleg quadrapod is not included in the model. Thus the actual structure should be somewhat stiffer than predicted by the computer model.

As is commonly done, the rms deviation of the reflecting surface from a best fit paraboloid is used as the measure of the antennas performance [5]. The displacement of the front nodes can be calculated for any elevation angle, but usually only the vertical and horizontal look deformation maps are calculated. For any other gravity vector orientation, the deformations are calculated as the appropriate linear superposition of these maps. This is rigorously correct for an elastic structure [2], but we found that linear superposition is accurate even when the effect of the nonlinear pin joint play is included. It is assumed that at each elevation the secondary mirror will be positioned to minimize the aperture plane phase error. The rms difference between the vertical and horizontal look maps, after removing the best fit paraboloid, provides a single number evaluation of the gravitational deformations and deviations from homology. The actual surface figure achieved can be significantly better than this if you pretune the surface for optimum performance over the most commonly used elevation range.

Optimization of the structural design was carried out by minimizing the deviations from homology consistent with loose constraints on the total weight and wind-induced distortions. Even in the days before work stations, the simple redundant geometry of the structure defined by only a few parameters allowed this optimization to be easily performed. The result is the backing structure described in the preceding section with the assigned weight classes given in Table 1. The elastic modulus, density, and thermal expansion coefficient are global parameters so that different construction materials could be easily explored. It was found that the performance goals could be met using an all-steel backing structure (except for the extruded aluminum spiders) so that more expensive and difficult to handle composite materials were not necessary. Figure 6 shows the predicted deviations from homology when the antenna moves from 90° to 0° zenith angle. The rms surface error for this map is 23 μm which is to be compared to a raw rms deformation of 288 μm. Thus the structure is 92% homologous.

The focal point for the best fit paraboloid shifts relative to the nominal focal point as a function of elevation. The best focus shifts 0.42 mm down and 0.80 mm towards the vertex as the reflector moves from the zenith to the horizon. The position of the secondary will also shift in response to the gravitational forces. The calculations of the deviations from homology assume that the secondary tracks this optimum position and the performance will degrade if the secondary is left in a fixed position. This can be minimized by optimizing the secondary position for an intermediate observing angle. The telescopes in the OVRO array suffer a maximum effective rms surface degradation of 60 μm over the full elevation range for a fixed secondary position.

The wind cross section is dominated by the panels. The gravitational deformation model with a zero weight backing

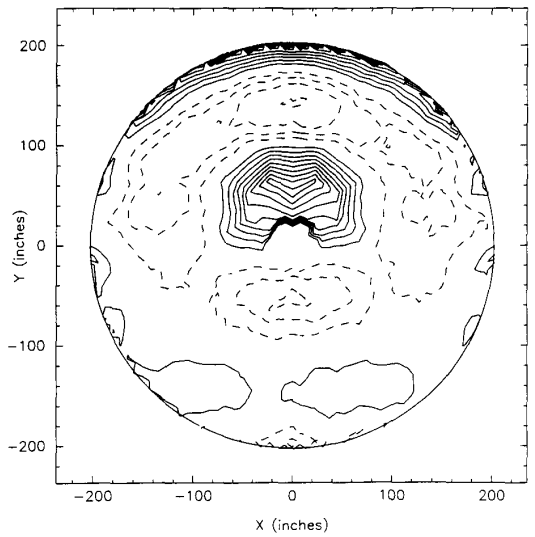

Fig. 6. Calculated deformation of the telescope surface between 0° and 90° elevation after removing the best fit paraboloid. The contour intervals are 10 μm with the 0 contour suppressed.

structure and panel weights proportional to the panel area normal to the wind direction was used to approximate the effect of wind. A face on wind is like the vertical look gravitational loading and wind blowing parallel to the aperture should be similar to the gravitational distortions calculated for the dish looking at the horizon. Thus the effect of wind can be approximated by adding a horizontal component to the gravity vector in the simulation program. In general, the less stiff and more homologous structures will suffer more from wind distortions. A prototype dish was constructed using much smaller cross-section members and although its gravitational deviations from homology were within the original design goals it suffered from excessive wind-induced distortions. The final design described in this paper meets much more stringent gravitational distortion specifications and suffers negligible wind distortion under normal operating conditions. For the worst case face on wind, the gravitational forces equal the wind forces for a wind speed of 75 km/h. The mount-drive motors do not supply sufficient torque for the antenna to track accurately at wind speeds above $\sim$ 40 km/h. Since the wind pressure scales as the velocity squared, under normal operating conditions wind-induced distortions are much less than the gravitational deformations.

The survival wind speed is an important issue for antennas operating on exposed mountain tops. The backing structure and panels are estimated to survive wind speeds up to 200 km/h at which point the panels will probably be blown away. The calculated maximum vertical load corresponds to a snow load of $\sim$ 1000 kg/m^2. The weakest components when looking at the horizon are the standoffs attaching the panels to the backing structure. A 100-mm-thick ice load can be supported in this orientation.

The effect of temperature gradients on an all-steel structure depends upon its general shape and only weakly upon the detailed geometry. Ideally, a structure made entirely from the same material will deform homologously for a uniform temperature change. In particular, the position of the secondary should move to compensate for changes in the focal length of the primary as long as the secondary support system is fabricated from the same material as the backing structure. The honeycomb aluminum reflector panels on the Leighton antennas are attached to the steel backing structure using 150-mm-long standoffs so expansion of the panels relative to the backing structure will not affect the large-scale surface figure.

The effects of different temperature distributions in the Leighton antenna structure have been analyzed using the computer modeling program. A gradient of 1 K across the 10-m-diameter produces only a 3-μm rms distortion. This is considerably less than the estimated distortion von Hoerner obtained for a simplified octahedron structure [3] and is a result of the flatter structure used here. A difference of 1 K between the spaceframe (including the feedlegs) and the mounting platform gives a 7-μm rms distortion. This last distortion is by far the most troublesome for antennas operating in an unprotected environment.

The difficult part is estimating reasonable values for the thermal gradients. The spaceframe structure for the Leighton telescopes is very open and is constructed of many small cross-section members. The estimated time constant is less than 1/2 h in winds greater than 5 km/h. (Daytime winds of less than 5 km/h are rare in the Owens Valley.) The measured temperature profiles show that despite diurnal temperature changes of greater than 20°C, with the maximum rate of change approaching 5°C/h, the gradients in the mounting platform and spaceframe are typically less than 1°C. The worst gradients are 5°C measured on clear winter days with winds of less than 5 km/h. Thus the calculated thermal distortions in the structure, based on measured gradients, are typically less than 10 μm rms with a worst case of 35 μm. The effective surface errors can be reduced by more than a factor of two if the large-scale temperature gradients are measured and the secondary moved to the optimum position.

The gravitational sag of the aluminum honeycomb panels is much less than the distortions caused by thermal gradients through the panels. The maximum panel sag is 18 μm at the center corresponding to 4 μm rms surface error. Optimizing the panel figure for the best average error over the full elevation range reduces the average surface error to 1 μm with a worst error of 2 μm rms. The curvature induced by a thermal flux of I W/m^2 through an all aluminum honeycomb panel is $c = M\alpha I/\kappa$, where α is the thermal expansion coefficient (2.3×10^{-5}°C^{-1} for aluminum), κ is the thermal conductivity (150 W/m°C for aluminum), and M is the inverse filling factor for the honeycomb (60 for the material used for the panels in the Leighton telescopes) [6]. Thus a flux of 1 W/m^2 through the panel produces a change in curvature of 10^{-5} m^{-1}. The sagitta for a 1-m-diameter panel will be $\sim$ 1 μm for a flux of 1 W/m^2.

The maximum solar heating flux is $\sim$ 1 kW/m^2 while the maximum radiative cooling to a cold night sky is $\sim$ 100

W/m^2 [7]. The actual fluxes depend upon the heat transfer efficiencies of the front- and back-panel surfaces. Wind obviously reduces the temperature gradients and improves the thermal performance of the panels as it does for the rest of the structure. It is difficult to decrease the solar spectrum absorptivity of the panels but the infrared emissivity of the front surface can be increased by using titanium dioxide paint so that the solar flux can be radiated back to the sky instead of transferred through the panel and radiated out the back. This helps the daytime performance but worsens the night-time radiative cooling to the sky. This approach was used for the telescopes used at OVRO. The maximum measured concavity for a panel painted with white titanium dioxide paint in full solar illumination is 120 μm corresponding to $\sim$ 20% of the solar flux flowing through the panel. The maximum measured convexity for radiative cooling to the cold night sky is 54 μm. The panel contributions to the rms surface error are 25 and 11 μm, respectively, for these two conditions.

The approach used for the CSO is to insulate the back of the panels with 13 mm of foam and leave the front surface unpainted. This optimizes the performance for night observations when radiative cooling is the dominant effect. The estimated flux through the panel, assuming a convective heat transfer to the air of 3 $W/m^2 \cdot K$ and surface emissivity of 5%, is reduced to less than 2 W/m^2. This produces an rms surface error of less than 1 μm. The average temperature of the panels is calculated to be an acceptable 1°C below ambient air temperature.

Table 2 lists all of the calculated contributions to the telescope surface errors for both the OVRO telescopes and the CSO telescope. This table also lists the estimated and measured fabrication errors discussed in the next section.

Table 2 Surface Error Budget*

	OVR typical, worst	CSO typical, worst
Environment		
Gravity	10, 17	10, 18
Thermal, spaceframe	10, 25	5, 10
Thermal, panels	11, 25	0, 1
Wind	3, 10	2, 5
Net environment	18, 40	11, 21
Fabrication		
Large scale		
Parabolic track	5, 10	2, 4
Fixture alignment	8, 10	4, 5
Lab temperature	5, 10	4, 5
Small scale		
Cutter scalloping	4, 5	2, 3
Panel front skin	4, 5	2, 3
Panel warp	4, 8	4, 6
Reassembly	8, 12	5, 8
Net fabrication	15, 24	9, 13
Net surface errors	23, 47	13, 21**

* All errors are rms surface errors in mm.
** The large scale fabrication and reassembly errors are not included in this number since the surface tuning process carried out at the CSO corrected these error, but a 5 mm measurement error is included.

V. Telescope Construction

The successful fabrication of a precision telescope requires that the physical structure closely match the characteristics assumed in the computer model. This is accomplished for the Leighton antennas by using pin joints and construction techniques which minimize the accumulated stress in the structure. The pin joints fastening the struts to the spider nodes at the ends of the post are arranged so that all of the forces at a node pass through the node point, as is assumed in the model, and thus avoiding the strength loss associated with bending moments at the joints. The structure is manufactured using precision components which also minimizes the stress.

The method for constructing the reflector described below produces a structure which can be built and accurately measured before shipping and installation. Because precision components are used, the telescope can be disassembled, shipped, and reassembled in the field with reasonable assurance that you will have a reflecting surface with the desired performance without having to undertake an extensive series of measurements and adjustments in adverse field conditions.

All of the members are manufactured to an exacting tolerance. As a tradeoff between manufacturing costs and the effects of accumulative errors, the manufacturing specifications very from $\pm$ 10μm for the length of the innermost members to $\pm$ 50μm at the rim. This corresponds to an accuracy of one part in 10^5 for the central members. This is better than can be achieved using standard machine-shop practices and special procedures were developed to economically achieve these tolerances.

The struts consist of tubular 1018 carbon steel tubes with the dimensions given in Table 1. The struts are cut to overall length and then the ends are slotted, annealed, and pressed flat with a gap to accept the thickness of the spider fins. The struts are then cleaned and plated. The precision holes for the pins are then machined into the ends of the strut. The machining is carried out in a shop whose temperature is controlled to $\pm$ 1°C. A Hewlett Packard model 5527A laser metrology system is used for measuring the hole spacing. There are typically six struts of each length. One hole is milled in one end of each strut. The mill is set up with a fixture to hold the strut with a locating pin through this milled hole. An undersized hole is milled at the nominal

location of the hole in the other end of one of the struts. The separation of the two holes in this strut is then measured using the measuring fixture. Any necessary correction to the hole spacing is dialed into the mill and a larger hole is milled into the strut. The strut is then remeasured and if it is within tolerance the hole is milled to full size. The rest of the struts in the batch are then machined and checked on the measuring fixture. Once the correct procedure is learned, one person can machine the precision holes to the necessary tolerances at the rate of 3 to 6 struts per hour.

The post and spider assemblies which comprise the front and back nodes and the connection between them present a different set of problems. Two or three precisely placed holes are required on each of six spider fins at each end of the assemblies. The posts are machined to length with a tolerance of $\pm$ 10μm on a lathe by interspersing small cuts with frequent measurements. A hole is bored in the spiders to accept the posts and the holes in the fins are machined by a four-axis CNC mill using the bottom of the bored hole as a reference. The CNC code used for this process is generated by the same module used to define the backing structure for the structure modeling program. The holes used for mounting the panels and for mounting the dish to the telescope mount are then machined in the outside ends of the spiders. The top and bottom spiders and the corresponding post are then placed in a fixture which holds the spiders tight to the ends of the post with the fins properly aligned while dowel pin holes are drilled to fasten the spiders to the post. The spiders and post are then disassembled, epoxy applied and reassembled with press fit pins. The overall hole to hole spacing is then verified using the metrology system. The struts and posts are dip-painted before being assembled into the backing structure.

There are many advantages to using precision components in the backing structure which justify this precision machining effort. The most important advantage is that such a structure can be disassembled and reassembled and still retain its original precision shape. The problem with assembly of imprecise parts is that the exact position of the nodes depends in detail how the stresses are propagated through the structure and thus on the exact details of how it is assembled. This is disastrous for a structure which is to be built and figured in the laboratory and then disassembled, transported to another site (such the top of a mountain or the moon), and then reassembled. Although it is often possible to refigure a surface after installation, this is a nontrivial and labor-intensive task even when carried out at a benign site at sea level. Assembling precision-machined components also introduces a minimum of unaccounted for forces. In particular, none of the members have to be forced or stressed anywhere near their elastic limit. Unless great care is taken, assembling a structure from imprecise parts will result in stressing some members (particularly around bolt or dowel pin holes) beyond their elastic limit. This weakens the structure. Even if the elastic limit is not exceeded, a large fraction of the designed stress margin can be lost and the structure can experience permanent deformation under environmental forces much less than predicted by the design model.

The Leighton dish backing structure can be assembled by one person without the use of a crane. This is because none of the members are longer than 1.5 m or heavier than 15 kg, the parts go together without having to apply large stresses, and the partially assembled structure holds its shape with the insertion of only a single pin at each joint. Assembly starts in the center and works outward. Triangular groupings of struts and posts are connected to the structure using undersized pins. When a group is complete, each joint is disconnected, a heat curing long pot-life epoxy (Scotch Weld 2214 manufactured by 3M) is applied, and reconnected using the full-sized press fit pins. Epoxy is not applied to joints which must be disassembled for shipping. The epoxy is heat-cured only after the structure is completely assembled. This ensures that there are no bending moments at the joints for the symmetrical vertical loading condition. The epoxy adds strength and removes the play from the pin joints. During this whole process the backing structure is kinematically supported on three bottom nodes which form an equilateral triangle with 2.29-m-long sides.

The panels are fabricated from a honeycomb sandwich which consists of two honeycomb cores and two aluminum sheets as shown in Fig. 4. The commercial honeycomb consists of the flat 1.3-mm-thick back sheet, a 51-mm-thick honeycomb back core, a flat 1.3-mm-thick middle sheet, and a 45-mm-thick honeycomb front core. The core has a 10-mm cell size and is fabricated from 0.076-mm-thick perforated aluminum foil. The elongated hexagonal shape panels are cut from this honeycomb material and 0.25-mm-thick aluminum edge skins are epoxied around the perimeter of each panel. Most of the panel strength is from the back core sandwiched between the middle and back sheets. The exposed front honeycomb core will be machined to the desired paraboloidal shape and the front reflecting aluminum sheet attached using the process described below.

The panels are connected to the top nodes of the space-frame by 150-mm-long standoffs as is shown in Figs. 4 and 5. The standoffs absorb the strain of the differential thermal expansion between the steel support structure and the aluminum panels. They are fabricated from 12.7-mm-diameter heat-treated 4140 steel with the top ends notched to minimize the bending moments transmitted to the panels. The standoffs are attached to the top node spiders using a differential nuts with a 3/4-in–16 outside thread to mate with tapped holes in the spiders and a 1/2-in–20 inside threads to mate with the threaded bottom ends of the standoffs. Nylon-tipped set screws are used to preload the threads to one side and remove any play. This gives a very rigid attachment and at the same time provides a smooth reproducible adjustment capability of 0.32 mm per turn. The corners of three surface panels meet at the top of the standoff where they are bolted to a 102-mm-diameter disc fastened to the standoff. The plates are bent to match the orientation of the flat back sides of the panels. There are

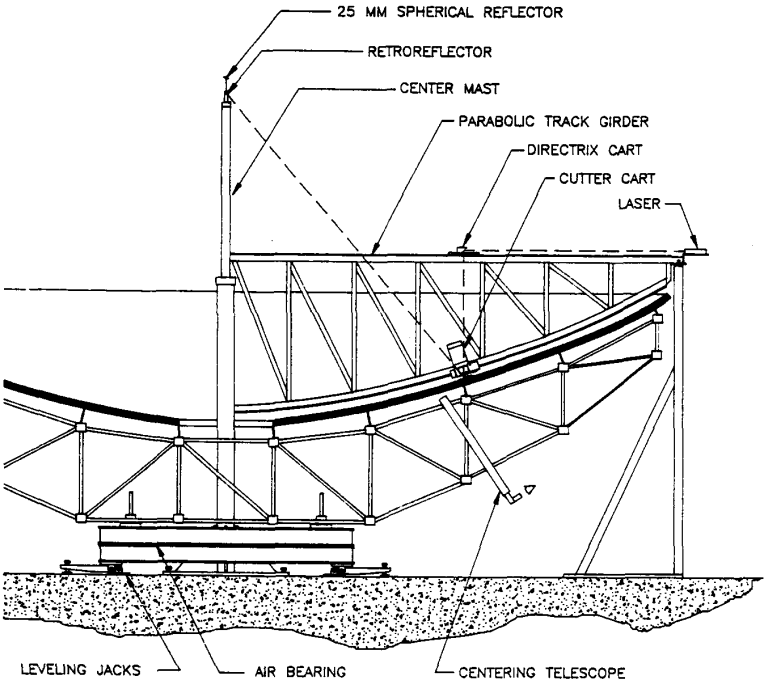

Fig. 7. Schematic drawing of the machine used to figure the telescope surface. The beam path for the laser distance measuring system is shown as a dashed line.

diamond-shaped plates at the corners of the panels which form the contact with the standoff discs. The construction proceeds by first bolting the diamond plates to the discs and then using epoxy to fasten the panels to the diamond plates. This procedure minimizes the strain at the connection between the top of the standoffs and the interface plates. A similar process is used at the neutral corners where three panels meet but are not connected to the backing structure. Thus the panels can be taken off and put back on without any significant loss in surface precision. This is part of the general strategy of keeping the dish stresses to a minimum in the vertical look orientation and making the assembly process reproducible.

The reflecting surface is figured in a unique process which involves treating the backing structure plus panels as a monolithic unit and cutting the desired parabolic shape into the exposed honeycomb core of the panels. This is done using a custom-built machining structure consisting of a 3.05-m-diameter air bearing and a 5.2-m-long parabolic track shown in Fig. 7. The cutter used to cut the honeycomb core rides on the track while the reflector structure rotates under the track on the air bearing. The surface is figured using many small cuts to minimize the heat dissipation. One of the major advantages of machining the reflecting surface shape into the exposed honeycomb core is that the low-density material can be cut with very little heat dissipation. The cutter is a 216-mm-diameter saw blade on a motor attached to a cart on the parabolic track. The blade is oriented to cut nearly parallel to the reflector surface to minimize the scalloping in the surface. It takes three weeks to make the rough cuts to within $\sim$ 3 mm of the final surface. At this point, the panels are removed for cleaning and sheet metal screws and additional epoxy are added to strengthen the connection between the panels and the diamond interface plates. The panels are then reattached to the spaceframe and temporary tensioning bars attached to the back of the panels are used to push the centers of the panels up a predetermined amount. This compensates for the measured elastic rebound which will occur when the front skins are epoxied to the machined honeycomb cores. The largest rebound is 110 μm. The air temperature and cutter power dissipation must be within narrow limits during the lengthy final few cuts. These take 12–24 h per pass during which time the air temperature must be stable to within $\pm$ 1°C and the power dissipation of the cutter motor less than 25 W. The cutting is stopped when a complete pass is deemed to have met all of the stringent temperature and alignment criteria discussed below. The estimated temperature induced errors during fabrication is less than 5 μm rms. The panels are then removed and the front 1.0-mm-thick aluminum skin is epoxied to the core using vacuum bagging to ensure that the skin conforms to the curvature cut into the core. The panels are then put back on the spaceframe and the surface figure verified by measuring its deviation from the parabolic template.

An advantage to machining the surface as single unit is that the cost is nearly independent of the number or shape of the panels. Also the number of adjustment points is reduced since neighboring panels are already aligned relative to each other. The Leighton reflectors consist of 84 panels but have

only 99 adjustable attachment points. This is particularly important when fine-tuning the surface in the field by hand or via an automated scheme.

The reflector is disassembled into manageable pieces and reassembled at the telescope site. The panels are removed and the backing structure is separated into sections for shipping. The structure is supported on 12 spring-loaded jack stands while three rows of top, diagonal, and bottom struts are removed to divide it into four 2 m wide by $\sim$ 10 m long sections. The backing structure is reassembled on a pad next to the mount using the spring-loaded jack stands to support the separate sections. A crane is then used to place the backing structure on the mount and it is bolted down at the same three nodes which supported the structure kinematically on the air bearing. The reflector for the CSO was assembled directly on the mount using a crane to support the backing structure sections. The panels are then put back on. At this point, the reflector experiences the same stresses as it had in the laboratory and the surface figure should be the same. The remaining six attachment nodes are bolted down using tapered shims and dial indicators to insure that these connections do not change the figure while pointing at the zenith. These connections, in the absence of wind, temperature, or feedleg stressed, do not carry any load when looking at the zenith, but do carry significant loads when the telescope is looking at the horizon. The feedlegs and secondary are then added to the antenna.

After the reflector is installed on the mount, the differential standoff nuts are adjusted to compensate for the weight of the feedlegs and to optimize the surface for the best performance over the full elevation angle range. These adjustments are based upon the computer model of the structure and amount to less than a 15-μm rms correction.

The accuracy of the final surface is determined by the quality of the machining fixture. The air bearing must provide a stable rotating platform with a well-defined rotation axis. The bearing is operated at 15 psi air pressure which produces a 7-μm-thick air gap when fully loaded with the 4900-kg reflector. The top half is constrained in the radial direction by four rollers. The bottom half is supported rigidly at three primary points. The backing structure is attached to the top half of the bearing at three points. It was found that the bearing halves were not sufficiently stiff to the two- and three-fold symmetric distortions and also had built-in low-order errors. The three-point bearing support was augmented by nine additional leaf springs effectively stiffening the bottom bearing half. A system of levers and weights was added to correct the shape of the top half of the bearing and to distribute the reflector's weight from the three primary mounting points to three additional points around the top bearing without disturbing the backing structure. Some of the alignment tools for the machining fixture are indicated in Fig. 7. Tilt meters or water manometers attached to the backing structure are used to verify that the air bearing rotates about a single vertical axis. A sighting telescope looking at a reflecting hemisphere mounted on the optical axis of the track parabola is used to measure the centering of the bearing. Additional information is obtained by monitoring the distortion of the bottom bearing half relative to the floor and of the top half relative to the backing structure. When the leaf springs and levers and weights are all properly adjusted the peak-to-peak deflections of the bearing halves are less than 5 μm.

The most difficult aspect of constructing the machining template is producing the parabolic track with an accuracy of better than 5 μm. The track girder actually consists of two precision tracks. The top directrix track is straight and level and the bottom parabolic track is surveyed relative to this directrix and a fixed focus. Various measuring devices can be mounted to a cart which rides on the directrix track. The initial setting of the directrix track was done using a microscope and laser system mounted on the cart to measure the distance to the surface of oil in a tray running the length of the track. Subsequent checking of the track is done using tilt meters (model 711 from Applied Geomechanics, Santa Cruz, CA) mounted on the cart or on a three-legged table slid along the track. The resulting directrix track is straight and smooth to an accuracy of $< 3\mu$m rms.

The problem of surveying the parabolic track reduces to a one-dimensional metrology problem when you utilize the fact that the distance from the focus to the surface and then to the directrix is a constant. The Hewlett Packard laser metrology system was used for this measurement. The laser head is mounted at the end of the directrix track with its beam pointed along the directrix track. The beam splitter and corner cube used for the reference beam is mounted on the directrix cart along with a pentaprism to turn the measuring beam exactly 90° down toward the parabolic track. A mirror is placed on the cutter cart which rides on the parabolic track at the same distance from the track that the final reflector surface will be. This mirror is oriented parallel to the track and directs the measuring beam from the pentaprism towards a corner reflector mounted at the focus. The beam then retraces its path back to the metrology laser head. The cutter cart is moved slowly along the lower track and the directrix cart is slaved to follow and keep the return laser beam centered in the beam splitter. The metrology system measures the change in distance from the directrix to the mirror on the cutter cart and then to the focus as a function of cart position. It thus measures the deviation of the path of the mirror from a parabola with a focus at the position of the corner reflector and a directrix parallel to the top track. The final rms deviation of the mirror path after careful alignment of the track is $< 4\mu$m.

The most stringent alignment requirements are in the plane of the parabola. A 0.25-mm displacement of the rotation axis of the air bearing relative to the optical axis of the parabola in this plane contributes a 5-μm rms error to the reflector surface. A 6 arcsec relative tilt of these two axes also results in a 5-μm rms error.

Temperature stability is very important for achieving the few ppm accuracy sought for the machining template and final surface accuracy. The high-bay shop used for the fabrication is the same one used for polishing the 5-m Hale optical telescope. The cork lined walls and ceiling provide

excellent passive temperature stability and less than 1°C diurnal temperature variation can be achieved.

VI. Surface Figure Measurements

The surface of the Leighton antennas have been measured using a variety of techniques. These include direct transducer measurements in the laboratory using the parabolic template, transducer measurements in the field, and holographic measurements using astronomical sources. The combination of these techniques measures the surface on scale sizes larger than 40 mm with an accuracy of ~ 5 μm.

The laboratory measurements are made using a noncontacting displacement transducer (made by Capacitec, Ayer, MA) mounted on the cutter cart which rides on the parabolic template used for machining the reflector. The sampling spacing is < 40 mm with each data point averaging over a 10-mm diameter. The surface roughness on scale sizes less than 10 mm is set by the ~ 2-μm finish on the commercial aluminum sheet used for the front skins. The measured rms deviation from the parabolic track is typically 10–15 μm. The measured change in the surface resulting from disassembling and reassembling the reflector in the laboratory is < 10 μm. This demonstrates that the construction and surface figuring process used for the Leighton antennas works extremely well. When all of the known sources of error are accounted for, the surface accuracy of the installed reflector is estimated to be 24 μm rms. These contributions are itemized in Table 2. The upper limit on the installed nighttime surface accuracy is 35 μm based upon holographic measurements using astronomical sources. This measurement includes the gravity, wind, and thermal distortions plus any imperfections in the secondary and beam transport optics.

The above errors are what has been achieved using our standard construction procedure. These errors were reduced considerably for the reflector installed at the CSO, also listed in Table 2. The adjustment of the parabolic template was improved to ~ 3 μm rms. The front skin sheeting was hand-selected for uniformity and surface quality. After completing the normal fabrication prodecure, several additional steps were undertaken to decrease the deviation from the template. A six-legged warping harness was added to the back of each panel so that corrections corresponding to the first seven Zernike deformations could be applied and 13-mm-thick insulation was added to the back of the panels to decrease the heat flux through them. The final step was the use a three-disc rotating sander mounted on the cutter cart to "polish" out the small-scale surface defects. These extra steps produced a surface with an estimated surface rms of 10 μm in the laboratory.

The primary measurement method for the telescope surface in the field is two-dish holography [8]. This technique measures the far-field voltage pattern of the antenna by using a reference antenna pointed at a point-like astronomical source and measuring the product of the voltages received by the reference antenna and the antenna being measured as it is scanned across the source. The aperture plane field

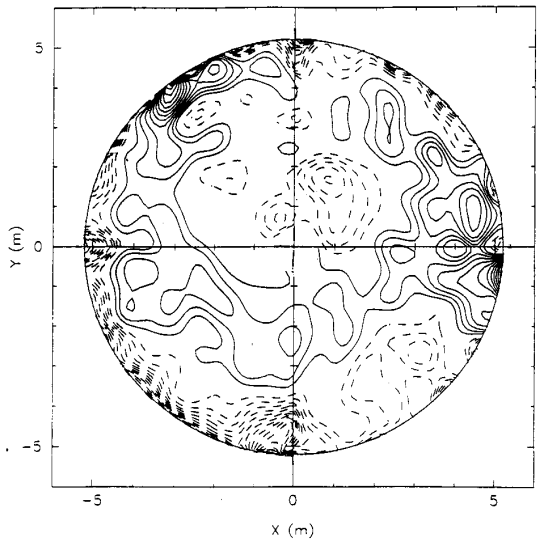

Fig. 8. A 27× 27 pixel holographic map of the surface of one of the antennas in the OVRO millimeter interferometer array obtained during a summer day using Venus as the radiation source. This is the surface figure achieved without any adjustments or corrections after assembly at OVRO and includes any errors that may be present in the secondary and beam transport optics. The contour intervals are 25 μm with the 0 contour suppressed and the rms aperture plane error is 46 μm.

pattern is then obtained from the Fourier transform of the far-field voltage pattern. The phase in the aperture plane is then converted to an effective surface figure. This is particularly convenient for the Leighton telescopes installed in the OVRO millimeter interferometer array since the primary data measured by an interferometer are the product of the voltages received by pairs of antennas. The resulting map is an absolute measurement of the aperture plane phase and includes the errors in the secondary mirror and the beam transport optics between the secondary and the heterodyne receiver. Figure 8 is a holographic map of the surface of one of the Leighton telescopes at OVRO using Venus as signal source. All five operational telescopes show similar surface figures with performance in good agreement with the error budget in Table 2.

A special holographic technique utilizing a shearing interferometer and a bolometric detector was developed for measuring the surface of the single CSO telescope in Hawaii [9]. The elevation-angle-dependent distortions have been studied by making maps of the surface as the celestial source is tracked across the sky [9], [10]. The measured deflections are in good agreement with the predictions of the computer model. The measured distortion in going from 30° to 74° elevation differs from the calculated distortion by less than 8 μm rms. The shearing interferometer measurements were used as the basis for fine tuning the CSO surface and a surface accuracy < 20 μm rms has been achieved.

The measurement of the thermal warping of the panels was done using holography at OVRO with Venus as a

source when it was close to the sun and comparing the maps with those obtained using night time sources. The mapping of the average warping of the panels is aided by the fact that the panels form a hexagonal tiling pattern in the aperture plane. Hence the average shape of the panels can be obtained by sampling the far-field beam pattern on a grid corresponding to the reciprocal lattice pattern of the hexagonal array. This is analogous to the X-ray diffraction determination of the structure factor for the unit cell in a crystal structure [11]. A transducer measurement system was also used to measure the small-scale errors of the CSO antenna and monitor the night-time radiative cooling effect on the panels. The results of these measurements are given in Table 2 and were discussed in Section IV.

VII. Summary

Robert Leighton's effort to develop an economical method for fabricating 10-m-class radio telescopes with diffraction-limited beams at submillimeter wavelengths has been very successful. The triangular spaceframe backing structure has proven to be very stiff and it deforms homologously under gravitational loading. The precision pin-joint construction has worked very well. The fabricated structure closely matches the assumptions used in the simple computer model and it can be disassembled and reassembled with little loss in surface accuracy. The relatively flat and very open spaceframe also behaves very well under thermal stress. It remains in equilibrium with the surrounding air and exhibits relatively small distortion for imposed thermal gradients.

The novel surface figuring machine works amazingly well. Converting the parabolic track setting problem to a one-dimensional measurement and rotating the reflector under the cutter solves a lot of the difficulties of figuring a large surface. Figuring the whole surface at one time removes the cost constraint on the quantity of panels and on the number of different panel shapes. Thus you are not limited to rings of pie-shaped panels. In addition, connecting all of the panels together into a membrane improves the mechanical properties of the reflector while reducing the number of adjustments required to fine-tune the surface figure.

Leighton's technique for figuring the panels involves cutting the honeycomb core, instead of solid material, thus greatly reducing the thermal distortion associated with making the panels. With only slight prestressing of the panels during the cutting process it was found that the aluminum sheets glued onto the figured panels very closely conformed to the desired parabolic reflector shape.

The whole fabrication process has been repeated reliably and with the same stringent specifications many times now. The structures show no evidence of degradation after 15 years of operation in the exposed high desert environment of the Owens Valley Radio Observatory. Telescopes with 35-μm surface accuracy can be routinely built and installed without the necessity of field setting of the panels. The performance can be improved to better than 20 μm by measuring and adjusting the surface in the field.

Acknowledgment

This paper would not have been possible without the many discussions Robert Leighton and the authors had over the course of many years. His patience and capacity to explain the physics of telescope structures was essential to the authors' ability to continue the fabrication and further the understanding of the Leighton telescopes. He repeatedly demonstrated that with a good understanding of the physics and attention to the relevant details you could solve most fabrication and measurement problems using relatively simple "homemade" instruments.

The authors also wish to thank the very competent and helpful staff at OVRO. Particular thanks goes to L. Wylie, C. Lackore, and S. Miller who worked extremely hard on fabricating and assembling the OVRO telescopes.

The CSO shearing interferometer was designed and built by Gene Serabyn and Eric Weisstein. They were also responsible for the CSO surface measurements used for the adjustments which were carried out by Anthony Schinckel.

References

[1] R. B. Leighton, "A 10-meter telescope for millimeter and submillimeter astronomy," Final Tech. Rep. for NSF grant AST 73-04908, 1978, 84 pages.

[2] S. von Hoerner, "Design of large steerable antennas," *Astron. J.*, vol. 72, pp. 35–47, 1967.

[3] ——, "Radio telescopes for millimeter wavelength," *Astron. Astrophys.*, vol. 41, pp. 301–306, 1975.

[4] J. W. Baars, "Technology of large radio telescopes for millimeter and submillimeter wavelengths," *Infrared and Millimeter Waves*, vol. 9. New York: Academic Press, 1983, pp. 241–281.

[5] J. Ruze, "Antenna tolerance theory," *Proc. IEEE*, vol. 54, pp. 633–640, 1966.

[6] J. Delannoy, "The design of high frequency antennas," in *Radio Interferometry: Theory, Techniques and Applications* (IAU coll. 131, ASP Conf. Ser., vol. 19), T. J. Cornwell and R. A. Perley, Eds. San Francisco, CA: Astronomical Soc. of the Pacific, 1991, pp. 15–25.

[7] J. D. Bregman and J. L. Casse, "A simulation of the thermal behavior of the UK-NL millimeter wave telescope," *Int. J. Infrared and Millimeter Waves*, vol. 6, pp. 25–40, 1985.

[8] P. F. Scott and M. Ryle, "A rapid method for measuring the figure of a radio telescope reflector," *Mon. Not. R. Astro. Soc.*, vol. 178, pp 539–545, 1977.

[9] E. Serabyn, T. G. Phillips, and C. R. Masson, "Surface figure measurements of radio telescopes with a shearing interferometer," *Appl. Opt.*, vol. 30, pp. 1227–1241, 1991.

[10] D. Woody, "Gravitational deflection of the Leighton telescopes," *Submillimetre Astronomy*, G. D. Watt and A. S. Webster, Eds. Amsterdam, The Netherlands: Kluwer, 1990, pp. 43–44.

[11] C. Kittel, *Introduction to Solid State Physics*, 3rd ed. New York: Wiley, 1966, ch. 2.

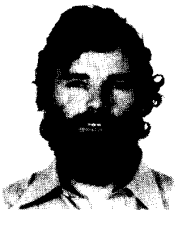

David Woody (Member, IEEE) received the Ph.D. degree from the Physics Department of the University of California at Berkeley in 1975. His thesis was on the measurement of the cosmic microwave background radiation in the frequency range from 50 GHz to 1 THz using a balloon-borne spectrometer. The instrument developed for this measurement used a He_3 cooled bolometer and a He_4 cooled Fourier transform spectrometer.

He became a research scientist at the California Institute of Technology, Pasadena, in 1978 where he worked on the development of the first superconductor–insulator–superconductor (SIS) heterodyne receiver. This receiver was used in Owens Valley Millimeter

Array. He was appointed a senior scientist and member of the professional staff at the Owens Valley Radio Observatory, Big Pine, CA, in 1981 where he continues to work. In addition to the development of millimeter-wave receivers for the interferometer array, he is responsible for the ongoing construction and performance of the 10-m-diameter antennas and their associated optics. He has published papers on a wide variety of instruments and observations related to millimeter and submillimeter astronomy.

David Vail has 23 years of experience in the fabrication of radio astronomy instruments. He has built and supervised the assembly and installation of six 10-m-diameter reflectors for the Owens Valley Millimeter Array and a refined version for the Caltech Submillimeter Observatory (CSO) on Mauna Kea, HI. He, together with Prof. Leighton, developed the techniques for fabricating and contouring the reflector panels. He designed and built the tooling for fabrication of backup structure struts, posts and spiders as well as the machines for surface refinement. He also participated in the assembly of the CSO dome and in the fabrication and integration of SIS receivers, bolometers and holographic instruments.

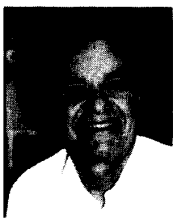

Walter Schaal received the B.S. degree in mechanical engineering from the California Institute of Technology, Pasadena.

He has been the senior mechanical engineer for the Owens Valley Radio Observatory (OVRO) and the Caltech Submillimeter Observatory (CSO) since 1982. He was responsible for the detailed design of the alt-az mount for the 10-m-diameter reflectors used at OVRO and CSO and the electro-hydraulic rail transporter used for the OVRO antennas. He also designed the CSO dome and door drive system, as well as SIS receiver tuners, beam choppers, and optical components for bolometer and holographic instruments. Recently he participated in the design of the Low Resolution Imaging Spectrometer and Polarimeter for the Keck telescope.

Mr. Schaal is a Registered Professional Engineer in the State of California.